

# Energy flows in vibrated granular media

Sean McNamara<sup>(1,2)</sup> and Stefan Luding<sup>(1)</sup>

(1) *Institute for Computer Applications 1, Pfaffenwaldring 27, 70569 Stuttgart, GERMANY*

(2) *Benjamin Levich Institute and Department of Physics, The City College of the City University of New York New York, NY 10031, USA*

(September 7, 2018)

We study vibrated granular media, investigating each of the three components of the energy flow: particle-particle dissipation, energy input at the vibrating wall, and particle-wall dissipation. Energy dissipated by interparticle collisions is well estimated by existing theories when the granular material is dilute, and these theories are extended to include rotational kinetic energy. When the granular material is dense, the observed particle-particle dissipation rate decreases to as little as  $2/5$  of the theoretical prediction. We observe that the rate of energy input is the weight of the granular material times an average vibration velocity times a function of the ratio of particle to vibration velocity. ‘Particle-wall’ dissipation has been neglected in all theories up to now, but can play an important role when the granular material is dilute. The ratio between gravitational potential energy and kinetic energy can vary by as much as a factor of 3. Previous simulations and experiments have shown that  $E \propto V^\delta$ , with  $\delta = 2$  for dilute granular material, and  $\delta \approx 1.5$  for dense granular material. We relate this change in exponent to the departure of particle-particle dissipation from its theoretical value.

46.10.+z, 05.60.+w, 05.40.+j

## I. INTRODUCTION

In this paper, we study granular materials where energy is provided by a vibrating plate [see Fig. 1(a)].

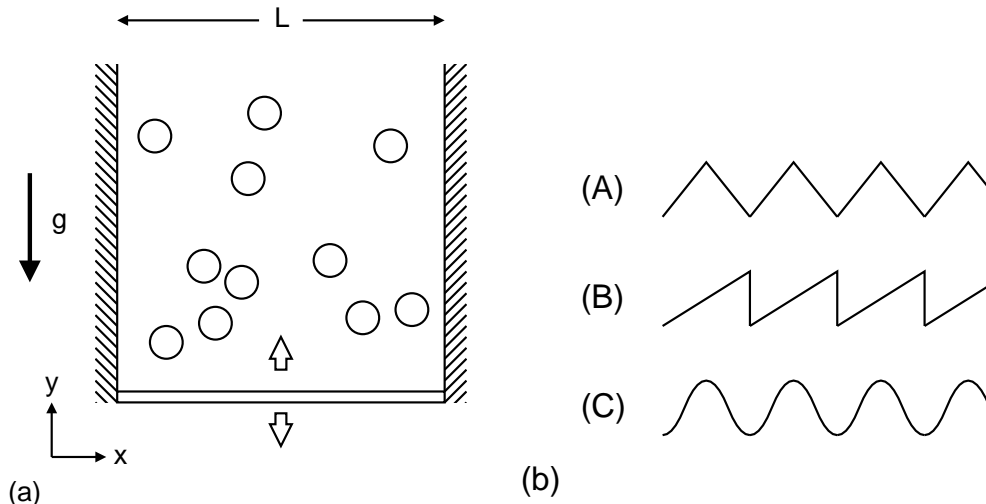


FIG. 1. (a) A sketch of the studied system. (b) The wave forms used to drive the vibrating plate.

In this system, two general classes of motion can be imagined, which we will name “coherent” and “incoherent”. In the first case, the particles move together in a coherent layer, bouncing at some frequency related to the vibration frequency. This state exhibits surface waves, and has been the subject of much recent work [1–3]. Another possibility is that the motion is incoherent. The particles remain suspended above the vibrating plate, with a density profile that – excluding fluctuations – remains constant throughout the vibration period. This second state has also been the subject of recent experiments, simulations and theories [4–10].

In this paper, we study this second type of motion. We search for a basic understanding of the physical processes which govern the input and dissipation of energy. This is a question of theoretical interest, because it provides a good test of kinetic theories of granular media. These theories, modeled after the kinetic theory of gases [11–13] have been shown to have quantitative success only for unforced granular media in the absence of gravity [12,14–16]. However, incoherent vibrated granular materials may be an experimentally accessible system well described by these theories. [7,8,13]

The paper is organized as follows. In Sec. II, we describe the studied system in detail and set forth our notation. In Sec. III, we review the literature. In Sec. IV, we check the previous results against our simulations, and construct some new theories. In particular, we examine five topics: 1) the rate of energy dissipation in particle-particle collisions, 2) the effect of particle rotations, 3) the energy input by the vibrating floor, 4) the energy dissipated by particle-wall collisions, and 5) the ratio of kinetic to gravitational potential energy. Finally, in Sec. V, we assemble the best theories and investigate the dependence of the energy on vibration velocity.

## II. DESCRIPTION OF THE SYSTEM

### A. Definitions

A sketch of the system is shown in Fig. 1(a). A granular medium, modeled by a gas of inelastic disks, is contained in a box of width  $L$  and infinite height. The gas is pushed against the bottom by a gravitational field with acceleration  $g$ . Energy is added to the system by the bottom of the box, which vibrates with period  $\tau$  and typical velocity  $V$ . (In Sec. IV C, we relate  $V$  to the maximum velocity  $V_{\max}$ .) The granular medium consists of  $N$  particles of radius  $a$  and mass  $m$ . Convenient nondimensional parameters describing the system are the length measured in particle radii, the number of layers of particles at rest  $H \equiv 2aN/L$ , and the number of particle radii a particle, initially at rest, falls during one cycle of a wall vibration,  $g\tau^2/(2a)$ . The description of the system is completed by specifying the particle-particle and the particle-wall collisions, and the wave form of the vibrating wall. We use the three wave forms shown in Fig. 1(b). Wave forms  $A$  and  $B$  are convenient for theoretical analysis [7,9,17], and wave form  $C$  is a computational convenient numerical approximation to a sine wave, constructed by patching together parabolas. In Sec. IV C, we will estimate the effect of this approximation on the energy input at the vibrating wall.

We consider collisions with constant normal and tangential restitution coefficients. This collision model has been widely studied and is relatively easy to analyze theoretically. The normal (tangential) restitution coefficient for collisions between particles is denoted  $r_p$  ( $\beta_p$ ), and for collisions between the particles and the side walls  $r_w$  ( $\beta_w$ ). The vibrating floor is elastic ( $r = 1$ ) and smooth ( $\beta = -1$ ). More details on the collision rule are presented in Appendix A.

We describe the state of the system with three types of energy, each defined per degree of freedom, per particle:  $\bar{E}$ , the translational kinetic energy of the particles,  $\overset{\circ}{E}$ , their rotational energy, and  $E_g$ , their gravitational potential energy. These energies are calculated as follows:

$$\bar{E} = \frac{m}{2N\bar{n}} \sum_{i=1}^N v_i^2, \quad \overset{\circ}{E} = \frac{mqa^2}{2N\overset{\circ}{n}} \sum_{i=1}^N \omega_i^2, \quad E_g = mg \frac{1}{N} \sum_{i=1}^N (y_i - h_0). \quad (1)$$

Here,  $v_i$  is the translational velocity of the  $i^{\text{th}}$  particle,  $\omega_i$  is its angular velocity, and  $y_i$  is its height above the time averaged position of the vibrating floor. The center of mass of the particles at rest is  $h_0$ . We calculate  $h_0$  from Eq. (14) of Ref. [5]. The number of translational (rotational) degrees of freedom per particle is  $\bar{n}$  ( $\overset{\circ}{n}$ ). In this paper, we consider exclusively two dimensional systems, where  $\bar{n} = 2$  and  $\overset{\circ}{n} = 1$ .  $\bar{E}$  and  $\overset{\circ}{E}$  are often called ‘‘granular temperatures’’. This terminology is not meant to imply that a thermal equilibrium exists in granular flows, but simply to draw an analogy between these quantities and the temperature of an ideal gas, which is proportional to the average energy per degree of freedom.

### B. General Approach

The ‘‘holy grail’’ of this paper are expressions for the energies  $\bar{E}$ ,  $\overset{\circ}{E}$ , and  $E_g$  in terms of the parameters  $L$ ,  $g$ ,  $V$ ,  $a$ ,  $\tau$ ,  $m$ ,  $r_p$ ,  $r_w$ ,  $\beta_p$  and  $\beta_w$ , together with a physical understanding

of the system. The starting point of the quest is the equation for the energy flow at steady state:

$$P_b = D_{pp} + D_{pw}, \quad (2)$$

where  $P_b$  is the power input by the bottom,  $D_{pp}$  is the power dissipated by particle-particle collisions, and  $D_{pw}$  is the power dissipated by particle-wall collisions. We will try to express each of these quantities in terms of  $\bar{E}$  and the system parameters. Then Eq. (2) will give an expression for  $\bar{E}$ , and we will also understand what processes determine  $\bar{E}$ .

In simulations, it is possible to monitor each of the three quantities in Eq. (2) or set each of them either to zero or to a known constant.  $D_{pp}$  can be set to 0 by using elastic particles, just as using elastic walls permits one to set  $D_{pw} = 0$ .  $P_b$  can be set to a known value by driving the bottom wall with waveform  $B$  [17]. We will discuss each of the three terms in Eq. (2) and exploit this separability to construct and verify our theories piece by piece.

### C. Simulational Approach

We use the standard event-driven method, which has been previously used to study vibrated granular materials [3,5,18,19]. Its main approximation is to consider that collisions are instantaneous, i.e. the time of contact during a collision is 0. The main disadvantage of event-driven simulations for granular materials is the occurrence of inelastic collapse – an infinite number of collisions occurring in a finite time [20,21]. To circumvent this problem, dissipation is turned off when the inelastic collapse singularity is approached. A similar method has been used in other recent work [3,19]. The fraction of dissipationless collisions is always less than  $10^{-4}$  for the simulations shown here. In addition, we repeated the three simulations that had the most dissipationless collisions, approaching more closely the inelastic collapse singularity, and found no measurable change

In the simulations presented here, we use the particle radius to define the unit of distance, and the particle mass to define the unit of mass. The unit of time is arbitrary. To apply our results to experimental systems, it is necessary to introduce conversion factors based on the particle mass and the particle radius, and to choose  $\tau$  and  $g$  so that  $g\tau^2/a$  has the same value as the experimental system.

In order to vary the system parameters in a consistent and organized way, the following procedure was used. First, ‘central’ values were selected for all the parameters except  $V$ . Then  $V$  is swept from small values to very large values, care being taken that all simulations fall within the “incoherent” category discussed above. The central values used in this paper are  $N = 160$ ,  $L = 50$ ,  $r_p = 0.95$ ,  $r_w = 1$ ,  $g = 1.0$  and  $\tau = 1.0$ . Then for each parameter, two series of simulations are run, one where the parameter is increased by a factor of 5, and another where it is decreased by a factor of 5. There are two exceptions:  $1 - r_p$  (not  $r_p$ ) is increased or decreased by a factor of 5, and  $g$  is increased or decreased by a factor of 25.

Most of the quantities measured during the simulations must be averaged over long periods of time to obtain stable results. To obtain a suitable averaging time, an “energy turn-over time”  $\tau_E = \bar{E}/P_b$  was estimated. The averaging time was taken to be  $20\tau_E$ . It was verified that the actual  $\tau_E$  was always close to the estimated one. Initial transients by running each simulation over several averaging periods, and verifying that averages were not changing significantly with time.

### III. REVIEW OF PREVIOUS WORK

#### A. Experiments and theory of Warr, et al.

Warr, Huntley and Jacques [7] modeled vibrated granular media as an isothermal “atmosphere”. By integrating over the “atmosphere”, one obtains

$$D_{pp} = 2(1 - r_p^2)NmgH(\bar{E}/m)^{1/2}. \quad (3)$$

Next, one can estimate the energy added by considering the density at the bottom of the “atmosphere”. The result for wave form  $A$  is

$$P_b = (1/2)NmgV^2(m/\bar{E})^{1/2}, \quad (4)$$

Setting  $P_b = D_{pp}$  yields

$$\bar{E} = \frac{mV^2}{4H(1 - r_p^2)}. \quad (5)$$

This result was calculated for smooth particles ( $\beta_p = -1$ ), with the system being driven by wave form  $A$ . The authors also present experimental results suggesting

$$\bar{E} \sim H^{-\bar{\nu}}V^{\bar{\delta}} \quad E_g \sim mgH^{-\nu_g}V^{\delta_g}. \quad (6)$$

with  $\bar{\nu} = 0.6 \pm 0.03$ ,  $\bar{\delta} = 1.41 \pm 0.03$ ,  $\nu_g = 0.27 \pm 0.11$  and  $\delta_g = 1.3 \pm 0.04$ . In contrast, the theory assumes that the gravitational potential energy is always proportional to the kinetic energy with  $\bar{\nu} = \nu_g = 1$  and  $\bar{\delta} = \delta_g = 2$ . Explaining the discrepancy between Eq. (5) and Eq. (6) was one of the major motivations for our study.

#### B. Simulations of Luding

Luding and co-workers have studied this problem with numerical simulations. Simulations without rotation [18] give  $\nu_g \approx 1$ ,  $\delta_g \approx 1.5$ . Simulations including rotation, carefully planned to duplicate the experiments [5] give  $\nu_g = 0.76 \pm 0.11$  and  $\delta_g = 1.60 \pm 0.10$ . When  $V$  is made very large and dissipation at the walls is suppressed [5,10],  $\delta \rightarrow 2$ . Lee [6] obtained results that are qualitatively similar. Luding [18] used a slightly different collision model which accounts for Coulomb friction. In the limit of infinitely strong friction, it reduces to the model used in this paper.

#### C. Theory of Kumaran

Kumaran [9] followed the same approach as Warr, Huntley and Jacques [7], except that he assumes that the particle velocities are distributed according to a Maxwellian velocity distribution. On the other hand, Warr, et. al assumed that all particles possess the mean velocity. Thus, Kumaran obtains the same results as Warr, et. al, except for the constant prefactor. Kumaran also investigates both wave forms  $A$  and  $B$ . He obtains

$$D_{pp} = \sqrt{\pi/2}(1 - r_p^2)NmgH(\bar{E}/m)^{1/2}, \quad \text{and} \quad (7a)$$

$$P_b = Nmg \left( \langle V \rangle + 2\sqrt{\frac{m}{\pi\bar{E}}}\langle V^2 \rangle + O(mV^3) \right), \quad (7b)$$

where the angle brackets indicate an average taken over one period. If a wave form is symmetric, like wave forms  $A$  and  $C$ , then  $\langle V \rangle = 0$ , and  $P_b \sim NmgV^2(m/\bar{E})^{1/2}$ , as in Eq. (4), but when the wave form is asymmetric (wave form  $B$ ), then the first term of the series is nonzero and dominant, so that  $P_b \sim NmgV$ .

## D. Theory and Simulations of McNamara and Barrat

McNamara and Barrat [17] studied the input of energy at a vibrating wall in the absence of gravity. They also found a difference between wave form  $B$  and wave forms  $A$  and  $C$ . For wave form  $B$ , the power input by the vibration wall is  $P_b = pVL$ , where  $p$  is the average pressure on the vibrating wall. This equation can be derived by considering the encounter of a single particle with a moving wall at time  $t_*$ . The particle's change in energy  $\Delta E$  is related to its change in momentum  $\Delta p$  by  $\Delta E = V(t_*)\Delta p$ , where  $V(t_*)$  is the wall velocity at time  $t_*$ . For wave form  $B$ ,  $V(t_*) = V$  always, so it is easy to average over time and find that the energy input is  $pVL$ . For wave forms  $A$  and  $C$ , the velocity of the plate is not always the same when the particles hit the plate. However, the probability of a particle hitting the plate at a given phase is governed only by the quantity  $U/V$ , where  $U$  is the velocity of the incoming particle. Therefore, for wave forms  $A$  and  $C$ ,  $P_b = pVLf(U/V)$ , where the function  $f$  is unknown. To adopt these results to a system under gravity, one sets  $pL = Nmg$ , the weight of the granular material. The result for wave form  $B$ ,

$$P_b = NmgV, \quad (8)$$

agrees with Eq. (7b) for asymmetric wave forms. For wave forms  $A$  and  $C$ ,  $P_b = NmgVf(U/V)$ , which coincides with Eqs. (4) and (7b) if  $f(U/V) = V/U$ .

## IV. RESULTS

### A. Particle-Particle dissipation of smooth particles

#### 1. Simulations

The two expressions for  $D_{pp}$  in Eq. (3) and Eq. (7a) differ only by a constant. We measure this constant by calculating

$$C_{pp} \equiv \frac{D_{pp}}{(1 - r_p)NmgH(\bar{E}/m)^{1/2}}. \quad (9)$$

Eq. (3) predicts  $C_{pp} = 4$  and Eq. (7a) predicts  $C_{pp} = \sqrt{2\pi} \approx 2.5$ . [The factor of 2 difference between the predicted values  $C_{pp}$  and Eqs. (3) and (7a) arises from replacing  $1 - r_p^2$  with

$2(1 - r_p)$ . For  $r_p \approx 1$ ,  $1 - r_p^2 \approx 2(1 - r_p)$ , so one might think that these two quantities would be equivalent. However, the difference at  $r_p = 0.75$  is sufficiently great to show that  $1 - r_p$  collapses the data better than  $1 - r_p^2$ .] Fig. 2 shows that the scaling successfully collapses the simulation data onto a single curve.

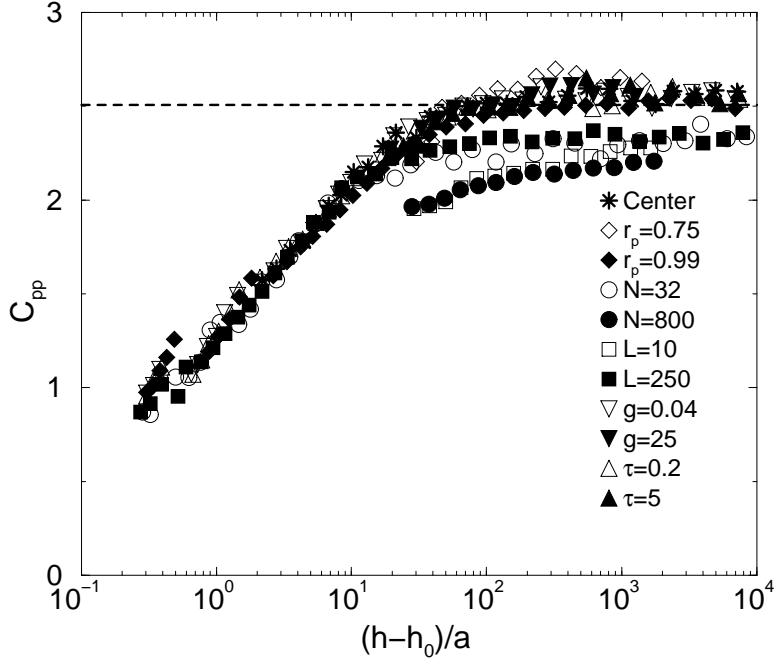


FIG. 2. A test of the scalings in Eqs. (3) and (7a). Here,  $C_{pp}$  is plotted against the height of the center of mass  $h \equiv N^{-1} \sum y_i$  above its position at zero energy,  $h_0$ . Both equations predict that  $C_{pp}$  should be a constant, which is indeed true for large heights (dilute granular media). The central simulation has  $N = 160$ ,  $r_p = 0.95$ ,  $L = 50$ ,  $g = 1$ , and  $\tau = 1$ ;  $V$  is varied over several orders of magnitude. The other series of simulations, each indicated by a different symbol, have the same parameters as the central one, except for the parameter shown in the legend. The bottom is driven with wave form  $B$ , and the side walls are replaced by periodic boundary conditions. The dashed line shows the constant predicted by Eq. (7a).

The figure can be divided into two regions: the dilute region,  $h - h_0 > 50a$ , and the dense region,  $h - h_0 < 50a$ . In the dilute region,  $C_{pp}$  is a constant, and quite close to the value predicted by Eq. (7a). The points collapse into families determined by the particular value of  $H = 2aN/L$  of each simulation. However, the scaling captures the dependence on  $V$ ,  $r_p$ ,  $g$  and  $\tau$  to within the noise in the simulations. In the dense region,  $h - h_0 < 50a$ , all simulations collapse tightly onto a curve  $C_{pp} \sim \log[(h - h_0)/a]$ . The reason for this dependence of  $C_{pp}$  on  $(h - h_0)/a$  is unknown. It is not due to the increasing density, because the low  $H$  ( $N = 32$  and  $L = 250$  curves in Fig. 2), as well as additional simulations (not shown) also collapse onto the same curve. Nor is the deviation due to waves propagating upwards from the vibrating plate; the agreement of the  $\tau = 0.2$  curve with the rest of the simulations excludes this. We also tried an alternate way of adding energy: the bottom plate is held fixed, and when a particle hits the bottom, it is given a velocity drawn from

a Maxwellian distribution. But these simulations also reproduce the curve shown in Fig. 2. Replacing periodic boundaries with elastic walls modifies only slightly Fig. 2.

Fitting a straight line to the points with  $a < h - h_0 < 50a$  (and excluding the  $N = 800$  and  $L = 10$  points) gives  $C_{pp} \approx 0.30 \log[(h - h_0)/a] + 1.35$ . This relation is valid over only about one and half orders of magnitude, so it is difficult to say whether it is really logarithmic, or whether the logarithm is only a convenient approximation.

## 2. A physical argument

We now derive the scaling relation from physical arguments. This permits us not only to understand why  $1 - r_p$  is better than  $1 - r_p^2$ , but also enables us to extend the theories to account for particle rotations and dissipation at the side walls.

From general kinetic theory arguments in the style of Haff [22], we argue that the dissipation due to collisions between particles will be

$$D_{pp} \sim N \langle \Delta E \rangle \left( \frac{U}{s} \right), \quad (10)$$

where  $\langle \Delta E \rangle$  is the average energy lost per collision,  $U$  is a typical particle velocity, and  $s$  is a typical particle separation. Multiplying  $\langle \Delta E \rangle$  by the collision frequency  $U/s$  gives the energy dissipation per particle per unit time. Then multiplying by the number of particles gives the total energy dissipation in the system.

Next, we must relate  $\langle \Delta E \rangle$ ,  $U$ , and  $s$  to  $\bar{E}$  and the independent parameters. First of all, Eq. (A9) in the appendix shows that  $\langle \Delta E \rangle \sim (1 - r_p^2) \bar{E}$  for smooth ( $\beta_p = -1$ ) particles. Next, since  $U$  is a typical velocity, we make the identification  $U \sim (\bar{E}/m)^{1/2}$ . Finally, to estimate the particle separation  $s$ , we turn to a one dimensional model. We imagine a column of  $n$  particles, suspended in a gravitational field by the vibrating plate at the bottom of the column. The column is in a steady state, so the net force due to collisions on each particle, averaged over time, must balance the gravitational force  $mg$ . Consider a particle somewhere in the column, with  $M$  particles above it ( $1 < M < n$ ). In a steady state, this particle must receive a momentum flux  $(M + 1)mg$  from the particle below it and transfer  $Mmg$  to the particle above it. The momentum transferred per collision is  $(1 + r_p)mU$ , and the collision frequency is  $U/s$ , hence the momentum flux will be proportional to  $m(1 + r_p)U^2/s$ . Equating the two expressions for the momentum flux

$$Mmg \sim (1 + r_p)mU^2/s, \quad (11)$$

and solving for  $s$  gives  $s \sim (1 + r_p)U^2/(Mg)$ .  $M$  will scale as  $n$ , and in two dimensions  $n$  can be approximated by the number of layers of particles  $H = 2Na/L$ . Again using  $U^2 \sim \bar{E}/m$ , we have  $s \sim (1 + r_p)\bar{E}/(mgH)$ .

Inserting our expressions for  $s$  and  $U$  into Eq. (10), we have

$$D_{pp} = C_{pp}(1 - r_p)NmgH(\bar{E}/m)^{1/2}. \quad (12)$$

This agrees in order of magnitude with the scaling tested in Fig. 2, and, in addition, explains why the  $1 - r_p$  of Eq. (9) collapses the data better than the  $1 - r_p^2$  of Eqs. (3) and (7a).

## B. Particle-particle dissipation for rough particles

All the simulations and theories presented so far in this paper consider “smooth” particles ( $\beta_p = -1$ ), thus ignoring rotation. But particles in granular flows rotate, and our theory would not be complete without considering rotation.

We now revise our argument for the scaling of  $D_{pp}$  in Sec. IV A, to take into account rotation. The only place the smoothness of the particles entered was in estimating the change in energy per collision  $\langle \Delta E \rangle$  in Eq. (10), so we use the more complicated expression given in the appendix, Eq. (A9):

$$\langle \Delta E \rangle = -2(1 - r_p^2)\bar{E} - \frac{q(1 - \beta_p^2)}{1 + q} \left( \bar{E} + \overset{\circ}{E}/q \right). \quad (13)$$

This involves  $\overset{\circ}{E}$  as well as  $\bar{E}$ , so we draw from a recent paper [23] on the ratio of translational to rotational kinetic energy in granular flows. One of the principle results of this paper is that

$$K \equiv \frac{\bar{E}}{\overset{\circ}{E}} = \frac{1 + 2q - \beta_p}{q(1 + \beta_p)}, \quad (14)$$

in vibrated granular flows. This convenient fact enables us to replace  $\overset{\circ}{E}$  with  $\bar{E}/K$ . The result is

$$\langle \Delta E \rangle = -2 \left[ (1 - r_p^2) + \frac{q(1 - \beta_p^2)}{1 + 2q - \beta_p} \right] \bar{E} = -2[1 - r_p^{*2}] \bar{E}. \quad (15)$$

with the “effective restitution coefficient”, governing the loss of energy,

$$r_p^{*2} = r_p^2 - \frac{q(1 - \beta_p^2)}{1 + 2q - \beta_p}. \quad (16)$$

Inserting  $\langle \Delta E \rangle \sim (1 - r_p^{*2})\bar{E}$  into Eq. (10) gives

$$D_{pp} = C_{pp}^{\circ} \left( \frac{1 - r_p^{*2}}{1 + r_p} \right) NmgH(\bar{E}/m)^{1/2}. \quad (17)$$

as the analogy of Eq. (12). This equation also defines a constant  $C_{pp}^{\circ}$ , in analogy with  $C_{pp}$ . We plot  $C_{pp}^{\circ}$  in Fig. 3.

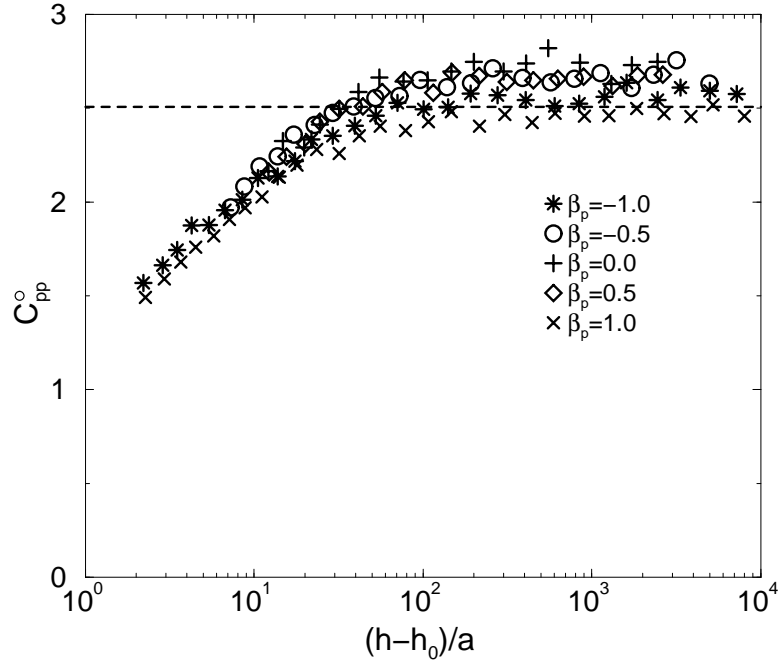


FIG. 3. A test of the scaling in Eq. (17), which defines  $C_{pp}^o$ . The parameters for the simulations are  $N = 160$ ,  $L = 50$ ,  $g = 1$ ,  $\tau = 1$ , and  $r_p = 0.95$ , with  $\beta_p$  given in the figure and  $V$  varied between 100 and 0.35. The dotted line and the  $\beta_p = -1$  simulation also appear in Fig. 2. Wave form  $B$  is used, and the side walls are replaced by periodic boundaries.

There remains a weak dependence on  $\beta_p$ , but  $C_{pp} = C_{pp}^o$  within the accuracy of the simulations.

### C. Energy input

We now turn our attention to the energy added by the vibrating floor. We test first the simplest result: Eq. (8), which applies only to wave form  $B$ . Reviewing all simulations shown in Fig. 2, we find the largest deviation from Eq. (8) is 1.6%, with most others much less (90% of the particles deviate by 0.5% or less). This equation is accurate because it is independent of the velocity distribution of the particles, and can be derived from the conservation of momentum [17].

For wave form  $A$ , Refs. [7,9] predict  $P_b \sim NmgV^2(m/\bar{E})^{1/2}$ . We test this scaling against the simulations in Fig. 4.

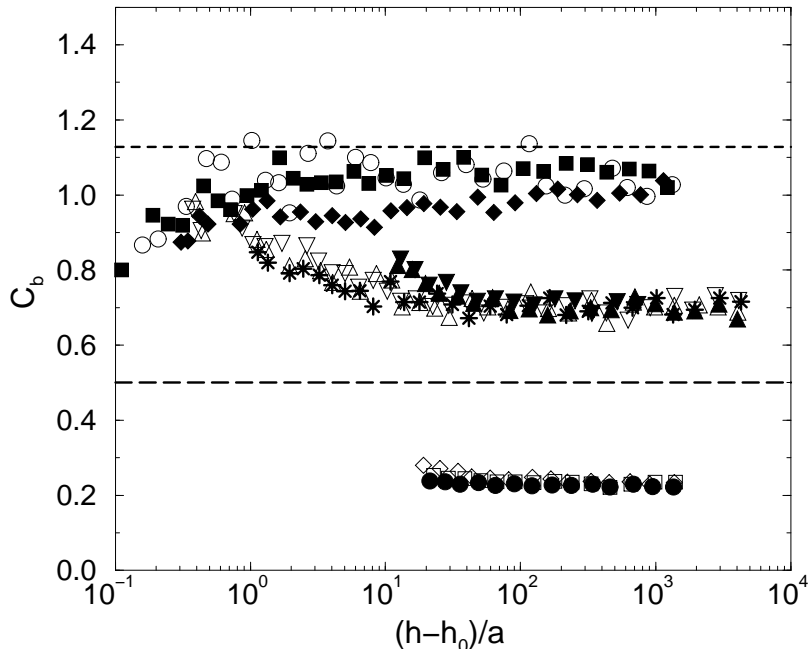


FIG. 4. A test of Eqs. (4) and (7a): we plot  $C_b \equiv P_b/[NmgV^2(m/\bar{E})^{1/2}]$  for the symmetric wave form  $A$ . The symbols and parameters of the simulations are the same as in Fig. 2, except the bottom plate is driven by wave form  $A$  instead of wave form  $B$ . The dashed lines show the constants predicted by Eqs. (4) and (7b).

We see that the scaling is only partially successful. The rescaled power input varies by as much as a factor of 5, and there is a strong dependence on  $H(1 - r_p)$  not captured by the scaling. An analogous plot for wave form  $C$  is similar.

To find a better way to calculate  $P_b$  for wave forms  $A$  and  $C$ , we try the scaling suggested by Ref. [17]:  $P_b = NmgVf(U/V)$  with  $U = (\bar{E}/m)^{1/2}$ . Let us now consider the unknown function  $f(U/V)$  in the limits  $U/V \rightarrow \infty$  and  $U/V \rightarrow 0$ . In the first limit, the particles are moving infinitely more quickly than the wall, and thus have an equal probability of hitting the wall when it is ascending or descending. In this case, the net energy input by the wall will be 0 because the energy gained by particles during the ascending phase is lost during the descending phase. As  $U$  becomes smaller, the particles have a higher probability to hit the wall during its ascending phase, and hence  $P_b$  becomes positive. Finally, in the limit  $U \rightarrow 0$ , the particles can hit the wall only during the ascending phase, so wave form  $A$  becomes equivalent to wave form  $B$ , so  $f(U/V) \rightarrow 1$ . This limiting value of  $f$  is also attained for wave form  $C$  if  $V = 2V_{\max}/3$ . In all cases,  $V$  is equal to a space average of the velocity of the plate during its ascending phase,  $V = A^{-1} \int_0^A V(y)dy$ , where  $y = A$  is the maximum height attained by the plate. When the plate sweeps through a motionless gas of particles,  $V$  is the average plate velocity seen by the particles (assuming all particles collide only once with the plate). For the sinusoidal wave form, a similar calculation gives  $V = \pi V_{\max}/4$ .

The unknown function  $f$  is shown in Fig. 5 for wave form  $A$ . An analogous plot for wave form  $C$  is similar.

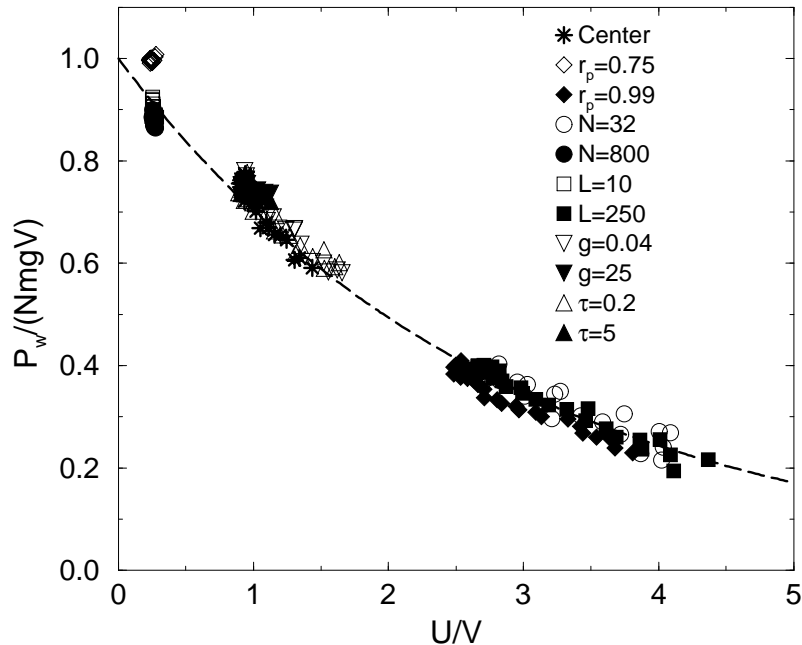


FIG. 5. A graph of  $f(U/V) = P_b/(NmgV)$ , with  $U = (\bar{E}/m)^{1/2}$ . The parameters and symbols of the simulations are the same as in Fig. 2, except that wave form *A* is used.

For wave forms *A* and *C*, points fall on a single curve, but they are bunched together depending on the value of  $(1-r_p)H$ . The function  $f$  is well approximated by an exponential, so that

$$P_b = NmgV \exp[-\alpha U/V]. \quad (18)$$

Least squares fits give  $\alpha_A = 0.353 \pm 0.002$ , and  $\alpha_C = 0.475 \pm 0.003$ . (Of course,  $\alpha_B = 0$ .) We note that  $\alpha_A/\alpha_C \approx 3/4$ . Fig. 5 does not prove that  $f$  is an exponential, because we have calculated  $f$  over less than one order of magnitude. However, an exponential is a better approximation for  $f$  than a power law or a straight line.

Note that in all scalings,  $P_b$  depends on the plate motion only through  $V$  and not through  $\tau$ . This differs from previous simulations, which suggest that  $P_b$  drops dramatically when  $\tau$  is below a critical value [4]. However, Ref. [4] used a soft sphere simulation method, where particles remain in contact during a finite time while colliding. If  $\tau$  approaches this contact time, the efficiency of the forcing will drop. On the other hand, if  $\tau$  is made very large, the granular material dissipates most of its energy during one vibration cycle, and the transition to the “coherent” state occurs. In the coherent state, the relevant parameter describing the forcing is no longer  $V$ , but the acceleration  $V/\tau$ .

#### D. Effect of Side Walls

Finally, we consider dissipation of energy through collisions between the particles and the side walls. There is no theory for  $D_{pw}$  in the literature. Nevertheless, we find that  $D_{pw}$  can be estimated by

$$D_{pw} = C_{pw}(v)D_{pp} \left( \frac{a}{L} \right) \left( \frac{\bar{E}_x}{\bar{E}} \right)^{3/2}, \quad (19)$$

where  $v \equiv (h - h_o)/(aH) = L(h - h_o)/(2Na^2)$  is proportional to the specific volume or inverse density.  $C_{pw}(v)$  is a linear function, and  $\bar{E}_x$  is the kinetic energy per degree of freedom in the  $x$  component of the particle velocities:  $\bar{E}_x = m(2N)^{-1} \sum v_{xi}^2$ . In a gas at thermal equilibrium,  $\bar{E}_x/\bar{E} = 1$ , but in these simulations,  $\bar{E}_x/\bar{E}$  can attain values as high as 0.2. The function  $C_{pw}(v)$  is shown with the data from the simulations in Fig. 6.

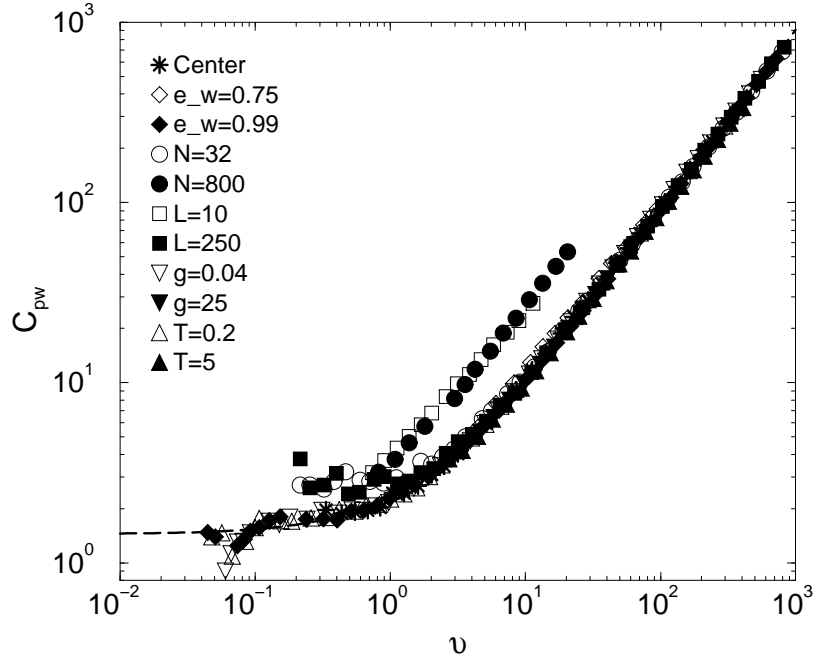


FIG. 6. A test of the scaling in Eq. (19), where  $C_{pw} \equiv (D_{pw}/D_{pp})(L/a)(\bar{E}/\bar{E}_x)^{3/2}$  is linear in  $v \equiv (h - h_o)/(aH) = L(h - h_o)/(2Na^2)$ . The dotted line is  $C_{pw} = 1.45 + 0.905v$ . These values were obtained by fitting all the points on the graph except those of the large  $H$  simulations ( $L = 10$  and  $N = 800$ ). These simulations have the same parameter values as those in Figs. 2, 4 and 5, except that periodic boundaries have been replaced by walls with  $r_w = r_p$  and  $\beta_w = -1$ .

The simulations agree well with Eq. (19), except for the large  $H$  ( $L = 10$  and  $N = 800$ ) simulations.

The result Eq. (19) can be understood as a continuation between two limits. In the limit of  $v \ll 1$ , Eq. (19) becomes  $D_{pw} \sim D_{pp}(a/L)(\bar{E}_x/\bar{E})^{3/2}$ . The factor of  $(\bar{E}_x/\bar{E})^{3/2}$  arise the  $x$  velocities alone determine the frequency of collisions with the wall, and the amount of energy lost. The factor of  $a/L$  appears because in this limit, the particles remain tightly packed, and rarely change places. The ratio between  $D_{pp}$  and  $D_{pw}$  will be equal to the ratio between the number of particle-particle contacts and the number of particle-wall contacts. Geometrical considerations show that these ratios are of order  $a/L$ .

In the limit of  $v \gg 1$ , Eq. (19) becomes [after using Eq.(7a) for  $D_{pp}$ ]  $D_{pw} \sim (1 - r_p^2)N\bar{E}_x^{3/2}/(m^{1/2}L)$ . Then, realizing that the average energy lost in particle wall collisions

is  $\langle E_w \rangle \sim (1 - r_w^2) \bar{E}_x$  (note that  $r_w = r_p$ ), and that the typical  $x$  velocity will be  $U_x = (\bar{E}_x/m)^{1/2}$ , Eq. (19) becomes

$$D_{pw} \sim N \langle E_w \rangle (U_x/L). \quad (20)$$

The similarity between this equation and Eq. (10) for  $D_{pp}$  permits the following interpretation: in the large  $h$  limit, the particles are bouncing back and forth between the two side walls. The factor  $U_x/L$  gives the frequency of collisions with the wall, so that  $\langle E_w \rangle (U_x/L)$  gives the rate of energy loss per particle. There are  $N$  particles, so a factor of  $N$  appears in Eq. (20).

The deviation of the large  $H$  simulations from Eq. (19) is probably due to their different mass distribution. These simulations differ from the others because they form a dense plug of particles suspended by a dilute “hot” region. In contrast, the others have a density maximum near the bottom, similar to a normal atmosphere. An additional curiosity is convection which appears in the large  $N$  simulations (solid circles in Fig. 6). Fig. 7 shows the motion of all the particles during one cycle for a  $N = 800$  simulation, revealing a circulation of particles within the plug. When  $V$  is decreased below a critical value, the circulation ceases, and this critical value of  $V$  corresponds to the break in the  $N = 800$  curve (solid circles) in Fig. 6. We have not studied this convection in detail.

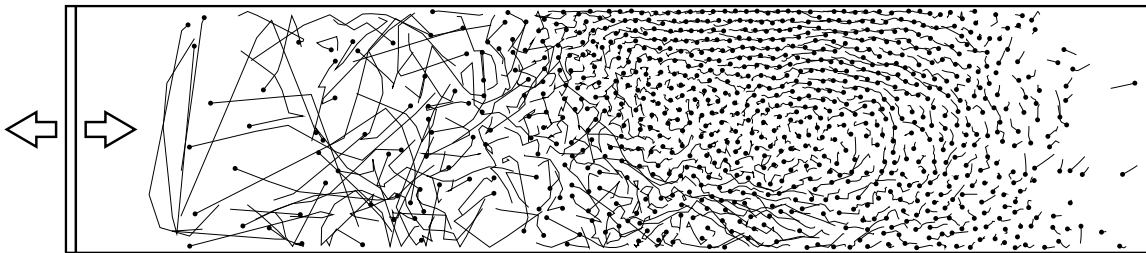


FIG. 7. Streaklines showing the motion of each particle during one cycle of the wall vibration. The solid dot shows the position of the particle at the beginning of the wall vibration, and the line shows its motion during the cycle. The simulation has  $N = 800$ ,  $r_p = r_w = 0.95$ ,  $\beta_p = \beta_w = -1$ ,  $L = 50$ ,  $g = 1$ ,  $\tau = 1$ , and  $V = 15.5$  with wave form  $B$ . The figure is horizontal, the vibrating bottom is on the left.

A further complication arises when the walls are rough ( $\beta_w \neq -1$ ). One must decide whether the walls move with the vibrating bottom or not; i.e. whether the bottom is a piston moving vertically between the stationary walls, or whether the particles are contained in a box which is shaken. If the side walls also move, then energy can be input at the side walls as well as at the bottom (i.e.  $D_{pw}$  can be negative) [5]. In this paper, we always consider the side walls to be stationary.

### E. Gravitational Potential energy

As shown in Sec. IV A,  $D_{pp}$  is a known function of the system parameters, the energy and  $h - h_0$ . We would like to eliminate this dependence on  $h - h_0$  before combining our

results for  $D_{pp}$ ,  $P_b$ , and  $D_{pw}$ . In order to do this, we plot in Fig. 8 the ratio  $\bar{E}/(r_p E_g)$  [where  $E_g \equiv mg(h - h_0)$  is the gravitational potential energy per particle].

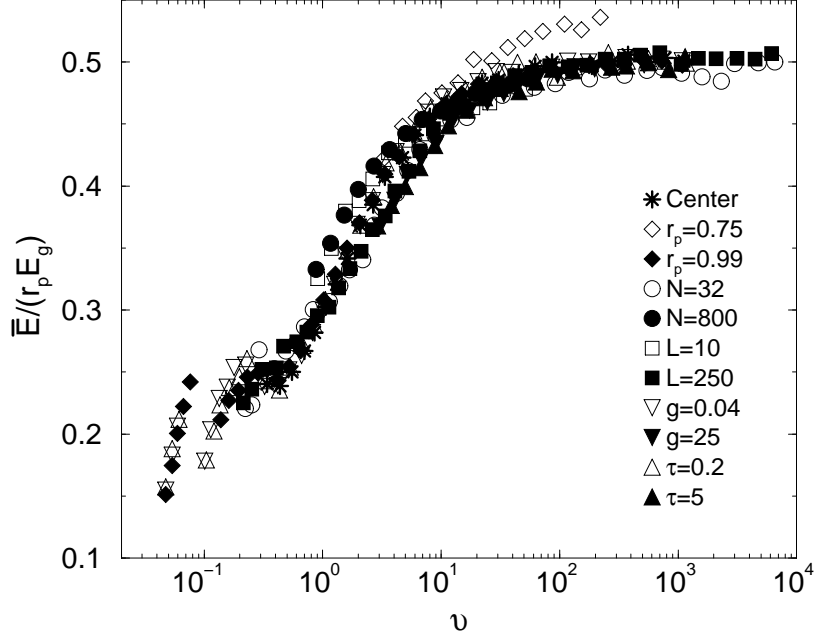


FIG. 8. The ratio of translational kinetic energy  $\bar{E}$  to gravitational kinetic energy  $E_g$  scaled by  $1/r_p$  and plotted against  $v \equiv (h - h_0)/(aH) = L(h - h_0)/(2Na^2)$ , for the simulations in Fig. 2.

This scaling successfully collapses the data onto a single curve reminiscent of Fig. 2. We note that  $h$  must be carefully calculated; if  $h$  is taken to be the height above the lowest position of the floor instead of the height above the average position of the floor, the simulations with  $g\tau^2 = 25$  fall off the curve.

Gravitational energy and kinetic energy are often assumed to be equivalent. Fig. 8 should be a cautionary note. The dependence of  $\bar{E}/E_g$  on the system parameters is quite complicated, and has not been theoretically investigated.

## V. SUMMARY AND TEST

To summarize and test the formulas for  $D_{pp}$ ,  $P_b$ , and  $D_{pw}$  presented in the previous sections, we calculate the predicted value of  $\bar{E}$  for a set of simulations from a previous paper [5]. Using Eqs. (17), (18) and (19) to rewrite the energy balance, Eq. (2), as an equation in terms of the system parameters and  $U = (\bar{E}/m)^{1/2}$ , gives

$$gV \exp(-\alpha U/V) = C_{pp} \frac{1 - r_p^{*2}}{1 + r_p} gHU + C_{pp} \frac{1 - r_w^{*2}}{1 + r_w} gHUC_{pw}(v) \left(\frac{a}{L}\right) \left(\frac{\bar{E}_x}{\bar{E}}\right)^{3/2}, \quad (21)$$

where  $C_{pp} = \min(0.30 \log[h - h_0] + 1.35, \sqrt{2\pi})$ , and  $C_{pw} = 1.45 + 0.905v$ . In writing down Eq. (21), we have assumed that Eq. (16) holds for the particle-wall restitution coefficients.

To close Eq. (21), expressions for  $(h - h_0)/a$  and  $\bar{E}_x$  need to be supplied. We assume  $(h - h_0)/a = 2\bar{E}/(mga)$  and  $\bar{E}_x = \bar{E}$ , which are true in a gas of elastic hard spheres under gravity ( $r_p = 1$ ,  $\beta_p = \pm 1$ ,  $V = 0$ ). These assumptions hold approximately for granular media, except in some extreme cases.

We test this equation against simulations in Fig. 9.

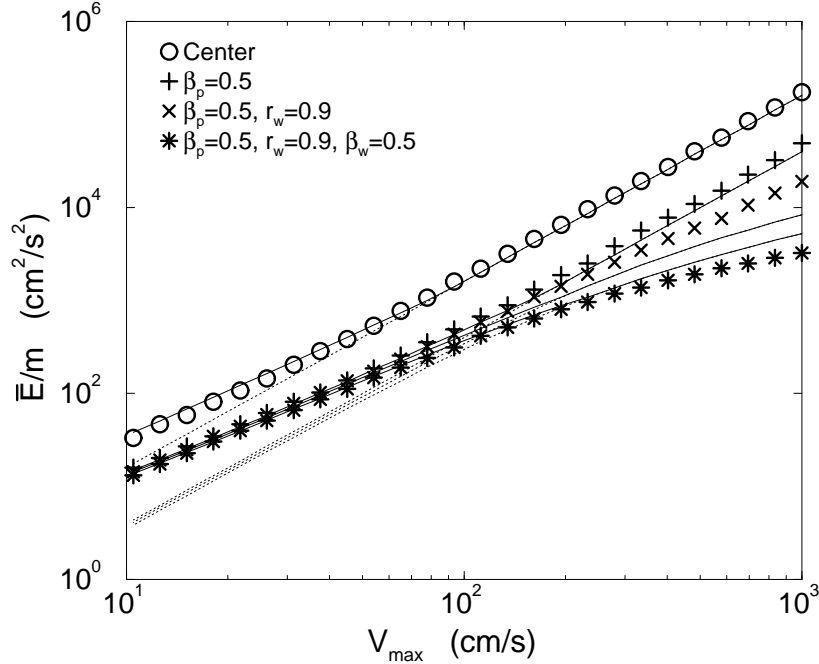


FIG. 9. A test of the theoretical results from Eq. (21). The central simulations have  $N = 50$ ,  $a = 0.05$  cm,  $L = 20a$ ,  $r_p = 0.9$ ,  $g = 981$  cm/s<sup>2</sup>,  $\tau = 0.01$  s,  $r_w = 1.0$ , and  $\beta_p = \beta_w = -1$ , with wave form  $C$ . The other simulations are the same, except for the parameters given in the figure legend. The solid lines give the results of the theory presented in Eq. (21). The dotted lines give the theory without taking into account the logarithmic dependence of  $C_{pp}$  on  $h - h_0$ , i.e., with  $C_{pp} = \sqrt{2\pi}$ .

The parameters of the central simulations are  $N = 50$ ,  $a = 0.05$  cm,  $L = 20a$ ,  $r_p = 0.9$ ,  $g = 981$  cm/s<sup>2</sup>,  $\tau = 0.01$  s,  $r_w = 1.0$ , and  $\beta_p = \beta_w = -1$ , with wave form  $C$ . These parameters were chosen to mimic the simulations in Fig. 11 of Ref. [5]. There remain three differences between these simulations and those of Ref. [5]. First, Ref. [5] uses a more complicated collision rule, where the tangential restitution coefficient varies between  $-1$  and an upper limit  $\beta_0$ , depending on the impact parameter. In our simulations, the tangential restitution coefficient is the same for all collisions. Secondly, Ref. [5] used slightly polydisperse spheres, whereas we use monodisperse spheres. Finally, we replace the sinusoidal wave form of Ref. [5] by wave form  $C$ . In spite of these differences, the simulations presented here show the same behavior as those of Ref. [5].

We show two versions of the theory, one which takes into account the logarithmic dependence of  $C_{pp}$  (the solid lines) and the other which does not (the dotted lines). The solid lines reproduce the observed dependence  $\bar{E} \sim V^{3/2}$  for  $V_{\max} < 100$  cm/s, whereas the dotted

lines show  $\bar{E} \sim V^2$ . Thus, the puzzling scaling observed in previous work [5,7] is due to the logarithmic dependence of  $C_{pp}$  on  $h - h_0$ . This dependence does not yet have a theoretical explanation.

For  $V_{\max} > 100$  cm/s, there is a significant disagreement for the simulations with dissipative walls ( $r_w \neq 1$ ), which can be traced back to the failure of the assumption  $\bar{E}_x = \bar{E}$ .

## VI. CONCLUSIONS

This paper has studied the two dimensional vibrated granular media, using the energy balance Eq. (2) to organize our investigation. Reviewing existing theories, we find the particle-particle dissipation is well understood in the dilute limit. We were able to show that Eq. (7a) is very accurate in the absence of side walls. This result was extended to deal with rough rotating particles with a constant tangential restitution coefficient. More work is needed to account for the more realistic situation of variable tangential restitution. In the dilute limit, particle-particle dissipation is well accounted for by existing theories, but in the dense limit, it shows an unexplained dependence on the height of the center of mass above the vibrating bottom,  $h - h_0$ , well approximated by a logarithm. It is this departure from the dilute theory which accounts for the  $E \sim V^{3/2}$  scaling observed in previous work. The cause of this departure is not yet known: it is not due to a change in density, since it depends only on the height of the center of mass. Nor can it be explained by waves propagating upwards from the bottom. Furthermore, the ratio between potential and kinetic energy,  $\bar{E}/E_g$ , can vary by almost a factor of 3. This variation is not understood, and hampers the ability of our theory to predict  $h - h_0$ .

The energy input by the vibrating plate is also well known for the special driving wave form  $B$  in Fig. 1(b). For more conventional wave forms, the energy input is well approximated by the exponentially decaying function of  $U/V$  shown in Eq. (18).

To our knowledge, this is the first paper to treat particle-wall dissipation in detail. Our theory accurately predicts energy losses at the wall, but requires knowing the difference between the horizontal and vertical kinetic energies. A more complete theory would have to estimate this difference from the system parameters.

We acknowledge the generous support of the Alexander von Humboldt-Stiftung and the DFG, SFB 382 (A6).

## APPENDIX A: THE COLLISION RULE

Consider a collision between two particles of radius  $a$ . Let  $\mathbf{v}_1$  be the translational velocity of the first particle,  $\boldsymbol{\omega}_1$  its angular velocity and  $\mathbf{r}_1$  its position at the time of contact. The quantities  $\mathbf{v}_2$ ,  $\boldsymbol{\omega}_2$ , and  $\mathbf{r}_2$  are the analogous quantities for the second particle. Then the relative velocity at the point of contact is

$$\mathbf{v}_c = \mathbf{v}_1 - \mathbf{v}_2 - a(\boldsymbol{\omega}_1 + \boldsymbol{\omega}_2) \times \hat{\mathbf{n}}. \quad (\text{A1})$$

Here, the unit vector  $\hat{\mathbf{n}} \equiv (\mathbf{r}_1 - \mathbf{r}_2) / |\mathbf{r}_1 - \mathbf{r}_2|$  points along the line connecting the centers of the colliding particles, from particle 2 towards particle 1. The change in the normal component of  $\mathbf{v}_c$  is parameterized by the ‘‘coefficient of normal restitution’’  $r_p$ , so that

$\mathbf{v}'_c \cdot \hat{\mathbf{n}} = -r_p(\mathbf{v}_c \cdot \hat{\mathbf{n}})$ , where the prime denotes the velocity after the collision. When  $r_p = 1$ , energy is conserved, and energy dissipation requires  $0 \leq r_p < 1$ . The coefficient of tangential restitution  $\beta_p$  is defined analogously, i.e.  $\mathbf{v}'_c \times \hat{\mathbf{n}} = -\beta_p(\mathbf{v}_c \times \hat{\mathbf{n}})$ . Energy is conserved for  $\beta_p = -1$  (perfectly smooth surfaces) and for  $\beta_p = 1$  (perfectly rough surfaces). In the first case the  $\boldsymbol{\omega}_i$  have no effect on outcome of the collision, and do not change during the collision. Energy is dissipated when  $\beta_p$  lies between these two extremes.

From the definitions of  $r_p$  and  $\beta_p$  and the assumption that the interaction takes place only at the point of contact, it is possible to derive the collision rules

$$\begin{aligned} \mathbf{v}'_{1,2} &= \mathbf{v}_{1,2} \mp \frac{1+r_p}{2} \mathbf{v}_n \mp \frac{q(1+\beta_p)}{2q+2} (\mathbf{v}_t + \mathbf{v}_r), \text{ and} \\ a\boldsymbol{\omega}'_{1,2} &= a\boldsymbol{\omega}_{1,2} + \frac{1+\beta_p}{2q+2} [\hat{\mathbf{n}} \times (\mathbf{v}_t + \mathbf{v}_r)], \end{aligned} \quad (\text{A2})$$

where the equation for particle 1 (2) takes the  $-$  ( $+$ ) sign in the top line above. To derive Eq. (A2) we used momentum conservation and the definitions

$$\begin{aligned} \mathbf{v}_n &\equiv [(\mathbf{v}_1 - \mathbf{v}_2) \cdot \hat{\mathbf{n}}] \cdot \hat{\mathbf{n}}, \\ \mathbf{v}_t &\equiv \mathbf{v}_1 - \mathbf{v}_2 - \mathbf{v}_n, \quad \text{and} \\ \mathbf{v}_r &\equiv -a(\boldsymbol{\omega}_1 + \boldsymbol{\omega}_2) \times \hat{\mathbf{n}}. \end{aligned} \quad (\text{A3})$$

Here,  $\mathbf{v}_n$  is the normal component of  $\mathbf{v}_c$ ,  $\mathbf{v}_t$  is the tangential component due to translation, and  $\mathbf{v}_r$  is the tangential component due to rotation. Note that  $\mathbf{v}_c = \mathbf{v}_n + \mathbf{v}_t + \mathbf{v}_r$ .

The change in translational energy is

$$\Delta \bar{E} = -Qv_n^2 - S [C_{t1}v_t^2 + C_{t2}(\mathbf{v}_t \cdot \mathbf{v}_r) - C_{t3}v_r^2], \quad (\text{A4})$$

with the positive prefactors  $Q \equiv m(1-r^2)/4$ ,  $S \equiv mq(1+\beta_p)/[4(1+q)^2]$ , and the constants  $C_{t1} \equiv 2+q(1-\beta_p)$ ,  $C_{t2} \equiv 2-2q\beta_p$  and  $C_{t3} \equiv q(1+\beta_p)$ . Likewise, the change in rotational energy is

$$\Delta \dot{E} = -S [-C_{r1}v_t^2 + C_{r2}(\mathbf{v}_t \cdot \mathbf{v}_r) + C_{r3}v_r^2], \quad (\text{A5})$$

where the constants are  $C_{r1} \equiv (1+\beta_p)$ ,  $C_{r2} \equiv 2(q-\beta_p)$ , and  $C_{r3} \equiv 2q+1-\beta_p$ . Note that the  $C$  are positive (only  $C_{r2}$  can also be negative) so that the signs in Eqs. (A4) and (A5) indicate the direction of energy transfer between the degrees of freedom.

Eqs. (A4) and (A5) can be added together to give

$$\Delta E = -Qv_n^2 - S(1+q)(1-\beta_p)(\mathbf{v}_t + \mathbf{v}_r)^2. \quad (\text{A6})$$

In this paper, we need to know the average energy lost per collision. Using angle brackets to denote averages over collisions, we have

$$\langle \Delta E \rangle = -Q\langle v_n^2 \rangle - S(1+q)(1-\beta_p)\langle (\mathbf{v}_t + \mathbf{v}_r)^2 \rangle. \quad (\text{A7})$$

Assuming that the particles' velocities are distributed according to a Maxwellian velocity distribution, and that their positions and velocities are uncorrelated gives

$$\langle v_n^2 \rangle = 8\bar{E}/m, \quad \langle (\mathbf{v}_t + \mathbf{v}_r)^2 \rangle = 4(\bar{E} + \dot{\bar{E}})/m, \quad (\text{A8})$$

in two dimensions. [23] Thus the total energy lost during one collision is

$$\langle \Delta E \rangle = -2(1 - r_p^2) \bar{E} - \frac{q(1 - \beta_p^2)}{1 + q} \left( \bar{E} + \overset{\circ}{E}/q \right). \quad (\text{A9})$$

- [1] F. Melo, P. Umbanhowar, and H. Swinney, *Phys. Rev. Lett.* **75**, 3838 (1995).
- [2] E. Clément, L. Vanel, J. Rajchenbach, and J. Duran, *Phys. Rev. E* **53**, 2972 (1996).
- [3] S. Luding, E. Clément, J. Rajchenbach, and J. Duran, *Europhys. Lett.* **36**, 247 (1996).
- [4] A. D. Rosato and Y. Lan, in *Powders & Grains 93*, edited by C. Thornton (Balkema, Rotterdam, 1993), p. 241.
- [5] S. Luding, *Phys. Rev. E* **52**, 4442 (1995).
- [6] J. Lee, *Physica A* **219**, 305 (1995).
- [7] S. Warr, J. M. Huntley, and G. T. H. Jacques, *Phys. Rev. E* **52**, 5583 (1995).
- [8] A. Goldshtein, M. Shapiro, L. Moldavsky, and M. Fichman, *J. Fluid Mech.* **287**, 349 (1995).
- [9] V. Kumaran (unpublished).
- [10] M. Müller, S. Luding, and H. J. Herrmann, in *Friction, Arching and Contact Dynamics*, edited by D. E. Wolf and P. Grassberger (World Scientific, Singapore, 1997).
- [11] J. T. Jenkins, *Arch. Rat'l. Mech. Anal.* **87**, 355 (1985).
- [12] C. K. K. Lun, *J. Fluid Mech.* **233**, 539 (1991).
- [13] A. Goldshtein and M. Shapiro, *J. Fluid Mech.* **282**, 75 (1995).
- [14] I. Goldhirsch and G. Zanetti, *Phys. Rev. Lett.* **70**, 1619 (1993).
- [15] S. McNamara and W. Young, *Phys. Rev. E* **53**, 5089 (1996).
- [16] P. Deltour and J.-L. Barrat, *J. Phys. I France* **7**, 137 (1997).
- [17] S. McNamara and J.-L. Barrat, *Phys. Rev. E* **55**, 7767 (1997).
- [18] S. Luding, H. J. Herrmann, and A. Blumen, *Phys. Rev. E* **50**, 3100 (1994).
- [19] S. Luding, in *Powders & Grains 97* (Balkema, Amsterdam, 1997).
- [20] B. Bernu and R. Mazighi, *J. Phys. A: Math. Gen.* **23**, 5745 (1990).
- [21] S. McNamara and W. R. Young, *Phys. Fluids A* **4**, 496 (1992).
- [22] P. K. Haff, *J. Fluid Mech.* **134**, 401 (1983).
- [23] S. McNamara and S. Luding, submitted (unpublished).